JBC ARTICLE

Dermatan sulfate epimerase 1 and dermatan 4-*O*-sulfotransferase 1 form complexes that generate long epimerized 4-*O*-sulfated blocks

Received for publication, May 14, 2018, and in revised form, June 11, 2018 Published, Papers in Press, July 5, 2018, DOI 10.1074/jbc.RA118.003875

Emil Tykesson[‡1], Antti Hassinen[§¶1], Katarzyna Zielinska[‡], Martin A. Thelin[‡], Giacomo Frati[‡], Ulf Ellervik[‖], Gunilla Westergren-Thorsson[‡], Anders Malmström[‡], Sakari Kellokumpu[§], and Marco Maccarana[‡2]

From the [‡]Department of Experimental Medical Science, Lund University, SE-221 00, Lund, Sweden, [§]Faculty of Biochemistry and Molecular Medicine, University of Oulu, 90570 Oulu, Finland, [¶]Institute for Molecular Medicine Finland (FIMM), University of Helsinki, 00014 Helsinki, Finland, and [‖]Department of Chemistry, Lund University, SE-221 00, Lund, Sweden

Edited by Gerald W. Hart

During the biosynthesis of chondroitin/dermatan sulfate (CS/DS), a variable fraction of glucuronic acid is converted to iduronic acid through the activities of two epimerases, dermatan sulfate epimerases 1 (DS-epi1) and 2 (DS-epi2). Previous *in vitro* studies indicated that without association with other enzymes, DS-epi1 activity produces structures that have only a few adjacent iduronic acid units. *In vivo*, concomitant with epimerization, dermatan 4-*O*-sulfotransferase 1 (D4ST1) sulfates the GalNAc adjacent to iduronic acid. This sulfation facilitates DS-epi1 activity and enables the formation of long blocks of sulfated iduronic acid–containing domains, which can be major components of CS/DS. In this report, we used recombinant enzymes to confirm the concerted action of DS-epi1 and D4ST1. Confocal microscopy revealed that these two enzymes colocalize to the Golgi, and FRET experiments indicated that they physically interact. Furthermore, FRET, immunoprecipitation, and cross-linking experiments also revealed that DS-epi1, DS-epi2, and D4ST1 form homomers and are all part of a hetero-oligomeric complex where D4ST1 directly interacts with DS-epi1, but not with DS-epi2. The cooperation of DS-epi1 with D4ST1 may therefore explain the processive mode of the formation of iduronic acid blocks. In conclusion, the iduronic acid–forming enzymes operate in complexes, similar to other enzymes active in glycosaminoglycan biosynthesis. This knowledge shed light on regulatory mechanisms controlling the biosynthesis of the structurally diverse CS/DS molecule.

One of the major glycosaminoglycans (GAGs)[3] in eukaryotes is chondroitin/dermatan sulfate (CS/DS). The initial step of the CS/DS biosynthesis is the formation of a protein–GAG linkage region, followed by formation of the polysaccharide backbone by addition of alternating D-glucuronic acid (GlcA) and *N*-acetyl-D-galactosamine (GalNAc) unit. After, or together with, polymerization, the chain modification process ensues by *O*-sulfation at position 4 or 6 of the GalNAc residues and by 2-*O*-sulfation of the uronic acid residues (1). In addition, GlcA residues can be epimerized at position 5 to form L-iduronic acid (IdoA) by two epimerases: dermatan sulfate epimerases 1 and 2 (DS-epi1 and -epi2) (2, 3). The epimerases share a highly conserved N-terminal epimerase domain but, in addition, DS-epi2 contains a putative C-terminal sulfotransferase domain with an unknown function (3). Dermatan 4-*O*-sulfotransferase 1 (D4ST1) selectively acts on IdoA regions of CS/DS, transferring a sulfate group from 3′-phosphoadenosine 5′-phosphosulfate (PAPS) to C4 of GalNAc present in IdoA-(1,3)-β-GalNAc-(1,4)-α-IdoA (4). In proteoglycans containing CS/DS, *e.g.* versican, decorin, biglycan, syndecan-1, CD44, serglycin, and endocan, the amount of GlcA compared with IdoA varies depending on the type of tissue and core protein (5). The importance of IdoA is clearly demonstrated in patients diagnosed with Ehlers-Danlos syndrome caused by loss-of-function mutations in *DSE*, encoding DS-epi1, or *D4ST1* who suffer from multiple organ disorders (6–8). CS/DS is also involved in processes such as the control of collagen fibril formation, cancer development, thrombin inactivation through heparin cofactor II (HCII), growth factor interactions, and migration (9–13).

Because the amount and localization of IdoA determine several functions of CS/DS, it is of utmost importance to understand factors that direct the formation of IdoA regions in the polymer. The amount of the three biosynthetic enzymes, as well as the concentration of the sulfate donor PAPS in the Golgi lumen, is a major regulatory mechanism (1) that affects both the sulfation degree and the chain length of CS/DS (14). It is reasonable to assume that the mechanisms of association between the enzymes determine the amount and structure of the final products. One general theme in GAG biosynthesis, as well as in other glycosylation pathways, is the physical interaction between enzymes working in consecutive reactions, which

This work was supported by the Medical Faculty at Lund University, Lund University, the Swedish Research Council, the Swedish Cancer Society Grant 140530 (to M. M.), the Mizutani Foundation for Glycoscience, the Greta and Johan Kock Foundation, the FLAK Research School, the Albert Österlund Foundation, the Royal Physiographic Society, and the Lars Hierta Foundation. The work was also supported by an Academy of Finland Grant and the Aaltonen Foundation. The authors declare that they have no conflicts of interest with the contents of this article.

[1] These authors contributed equally to this work.

[2] To whom correspondence should be addressed: BMC C12, 22184, Lund, Sweden. Tel.: 46-0-462228574; E-mail: marco.maccarana@med.lu.se.

[3] The abbreviations used are: GAG, glycosaminoglycan; DS-epi1, dermatan sulfate epimerase 1; DS-epi2, dermatan sulfate epimerase 2; D4ST1, dermatan 4-*O*-sulfotransferase 1; GlcA, D-glucuronic acid; GalNAc, *N*-acetyl-D-galactosamine; IdoA, L-iduronic acid; CS/DS, chondroitin/dermatan sulfate; PAPS, 3′-phosphoadenosine 5′-phosphosulfate; qRT-PCR, quantitative RT-PCR.

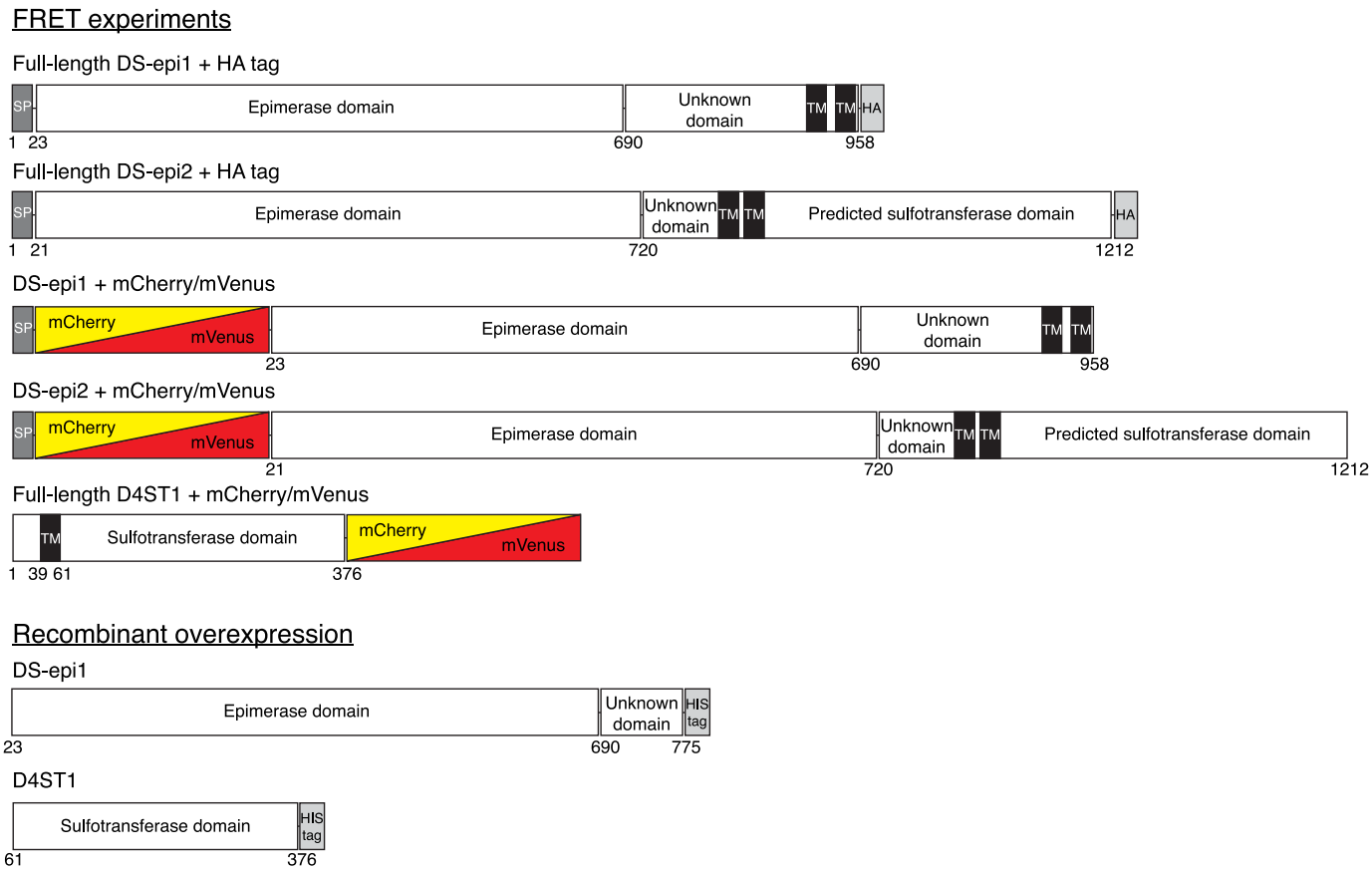

Figure 1. DS-epi1, DS-epi2, and D4ST1 constructs.

thus become linked and kinetically favored in the competition with other possible reactions (15).

Our hypothesis is that the interplay between DS-epi1, DS-epi2, and D4ST1 regulate the amount and distribution of IdoA in CS/DS. We have explored this potential physical interaction by FRET, immunoprecipitation, and cross-linking experiments and verified the functional effects by *in vitro* enzymatic investigations.

Results

DS-epi1 epimerase activity is enhanced when co-incubated with D4ST1

The necessity of both DS-epi1 and D4ST1 for the formation of long IdoA blocks is well established (16, 17). In this report, we investigated the mechanisms behind this functional collaboration. First, the combined action of the two recombinant enzymes (see Fig. 1 for the utilized constructs) was reconstituted *in vitro*. The first step in the epimerization reaction by DS-epi1 is abstraction of a proton from C5 of GlcA, followed by addition of a proton from the opposite side of the sugar plane, forming IdoA (18). The abstracted proton is subsequently released into the medium as water. In our assay, epimerase activity was followed by the release of tritiated water formed upon incubation with C5-^{3}H-radiolabeled chondroitin. When incubated alone, DS-epi1 showed a linear rate of formation of tritiated water (Fig. 2*A*). Co-incubation with D4ST1, after lag phase, increased the rate of epimerase activity by approximately five times.

Co-incubation of DS-epi1 and D4ST1 forms long stretches of repeating IdoA–GalNAc–4S structures

D4ST1 sulfates the C4 hydroxyl group of GalNAc only when adjacent to IdoA. To follow the sulfation reaction performed by D4ST1 in the presence of DS-epi1, polysaccharide products were depolymerized with chondroitinase ABC, which degrades both GalNAc–GlcA and GalNAc–IdoA linkages. The resulting disaccharides were labeled with the fluorophore 2-aminoacridone and analyzed by HPLC. Only two types of disaccharides were detected, *i.e.* unsulfated ΔUA–GalNAc and the mono 4-*O*-sulfated ΔUA–GalNAc–4*S*, formed with a kinetic similar to the release of tritiated water (Fig. 2*B*).

To analyze the spatial distribution of the IdoA–GalNAc–4*S* moieties in the polymer, products of D4ST1/DS-epi1 co-incubations were degraded with chondroitinase AC-I and -II, which cleave only GalNAc–GlcA linkages, allowing the analysis of the untouched IdoA-containing structures. PAP^{35}S was used in the incubations, enabling the analysis of the sulfated products by scintillation counting. At an early time point (45 min), when the sustained epimerase and sulfotransferase activities had just begun, the major products were tetrasaccharides, hexasaccharides, and octasaccharides, corresponding to one isolated or two or three adjacent IdoA residues, respectively (Fig. 2*C*). At a later time point (75 min), larger structures eluting at the void volume of the column were present in addition to the shorter structures, which did not change with time.

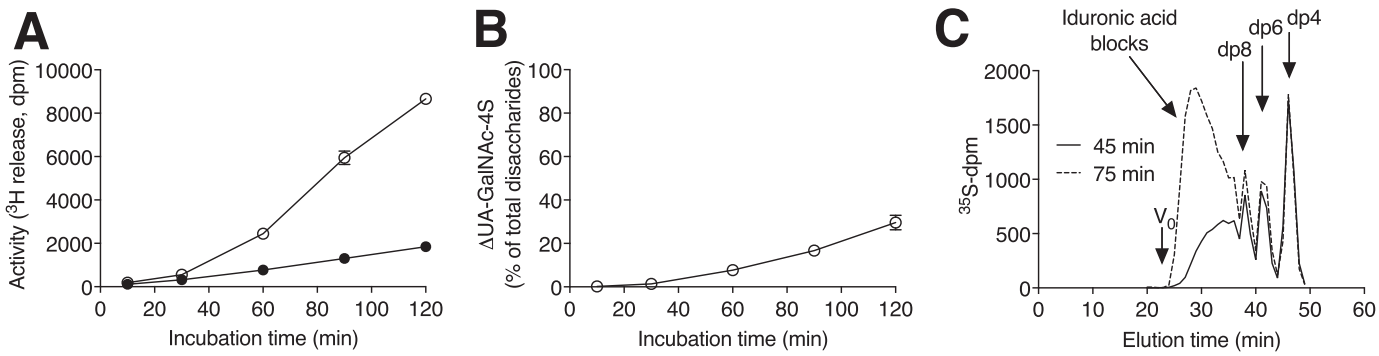

Figure 2. **Co-incubation of D4ST1 with DS-epi1 increases the epimerase activity and results in formation of long iduronic acid blocks.** *A*, DS-epi1 alone (*filled circles*) or in combination with D4ST1 (*empty circles*) was incubated with C5-^{3}H-chondroitin. Epimerase activity was measured by the release of tritiated water. *B*, disaccharide fingerprint of D4ST1/DS-epi1 co-incubation products. The mono 4-*O*-sulfated ΔUA-GalNAc-4*S* disaccharide is shown as percentage of the total polysaccharide. *C*, size determination on Superdex Peptide of the products formed by incubation of C5-^{3}H-Ch with DS-epi1, D4ST1, and PAP^{35}S after chondroitinase AC-I and -II degradation. Products were isolated after 45 (*solid line*) and 75 (*dotted line*) min of incubation. Eluted fractions were analyzed by scintillation counting of ^{35}S. The peak representing the excess PAP^{35}S, eluting after dp4, is not shown. V_0 represents the void volume of the column.

Colocalization of endogenous DS-epi1 and D4ST1 in the Golgi apparatus revealed by confocal microscopy

Confocal microscopy of endogenous enzymes was used to verify the presence of a close spatial arrangement of D4ST1 and DS-epi1. The epithelial non–cancer-derived MCF 10a cell line was chosen as a target because of its high concomitant expression of DS-epi1, DS-epi2, and D4ST1, as assessed by quantitative RT-PCR (qRT-PCR) and Western blotting (Fig. 3, *A* and *B*). Confocal images revealed the colocalization of DS-epi1 and D4ST1 in the Golgi complex, supported by a high-resolution line scan (Fig. 3, *C* and *D*). The colocalization of DS-epi1/D4ST1 was also observed with the overexpressed FRET constructs in COS-7 cells (Fig. 4*B*).

DS-epi1, DS-epi2, and D4ST1 form homomeric and heteromeric complexes

To determine whether these three enzymes interact and form heteromeric and functionally relevant complexes in live cells, we first confirmed the correct localization of the enzymes in the Golgi of COS-7 cells. Expression plasmids with FRET enzyme constructs tagged with either mVenus or mCherry fluorescent proteins were prepared (Fig. 1) and the subcellular location of the expression products was analyzed by fluorescence microscopy. All six mVenus and mCherry (not shown) enzyme constructs overlapped with the GM130 Golgi marker (Fig. 4*A*). We also evaluated the colocalization of the enzymes in the Golgi membranes by expressing selected enzyme pairs (Fig. 4*B*). The measured average overlap coefficients were 0.73 ± 0.02 for DS-epi1/DS-epi2, 0.69 ± 0.05 for DS-epi1/D4ST1, and 0.68 ± 0.03 for DS-epi2/D4ST1, confirming their similar distribution in the Golgi (Fig. 4*C*).

Next, we used high-content imaging for FRET measurements of enzyme interactions (Fig. 4*D*, *right*). Interestingly, the results show that DS-epi1 interacted with both DS-epi2 and D4ST1. The corresponding FRET signals were 60 ± 5% (mean ± S.D.) and 27 ± 3% of the positive control, respectively. Cotransfection of the FRET constructs together with the competing HA-tagged DS-epi1 construct showed that both interactions were markedly inhibited by this non–FRET-compatible construct. Thus, the results show that the observed interactions are specific and governed by the enzymes themselves. However, DS-epi2 did not interact with D4ST1. The fact that HA-tagged DS-epi2 significantly inhibited the interaction between DS-epi1 and D4ST1 is also consistent with its binding to DS-epi1. In addition, we also observed that each enzyme formed homomeric complexes (Fig. 4*D*, *left*) in live cells in the absence of a heteromeric counterpart, as also noted previously for other Golgi localized enzymes (for a review see Ref. 15). All of the homomeric interactions were inhibited by the HA-tagged DS-epi1 construct, confirming that DS-epi1 interacts not only with itself but also with DS-epi2 and D4ST1. Taken together, these data show that the two epimerases, when co-expressed, form a heteromeric complex and that only the DS-epi1 epimerase is able to interact with the D4ST1 sulfotransferase.

The FRET results were corroborated by immunoprecipitation experiments. The three enzymes were co-overexpressed in COS-7. An anti-D4ST1 antibody could pull down DS-epi1 and DS-epi2 (Fig. 5*A*). This result, together with the FRET data, reveals the existence of a higher order complex which consists of DS-epi1, DS-epi2, as well as D4ST1.

Next, after individual overexpression of the three enzymes, the intact COS-7 cells were exposed to the membrane-permeable cross-linker disuccinimidyl suberate. Western blotting detection showed formation of complexes ranging from 250 kDa to more than 500 kDa, with parallel disappearance of the monomeric enzymes (Fig. 5*B*, *right panels*). In the chosen conditions, only a minority of the cellular proteins were cross-linked, as seen in the total lysate analysis (Fig. 5*B*, *left panels*). These complexes most likely represent heterocomplexes between the overexpressed and endogenous enzymes, as well as homocomplexes of the overexpressed proteins.

In summary, FRET, immunoprecipitation, and cross-linking data indicate the presence of homocomplexes and heterocomplexes of the three enzymes, given the capability of DS-epi1 to interact with DS-epi2 and D4ST1.

Effect of DS-epi2 down-regulation on biosynthesis of iduronic acid

The interaction of DS-epi2 with DS-epi1, potentially interfering also with the DS-epi1/D4ST1 complex, further poses the question of the functional role of DS-epi2 in IdoA biosynthesis. To investigate that, DS-epi2 was efficiently down-regulated by

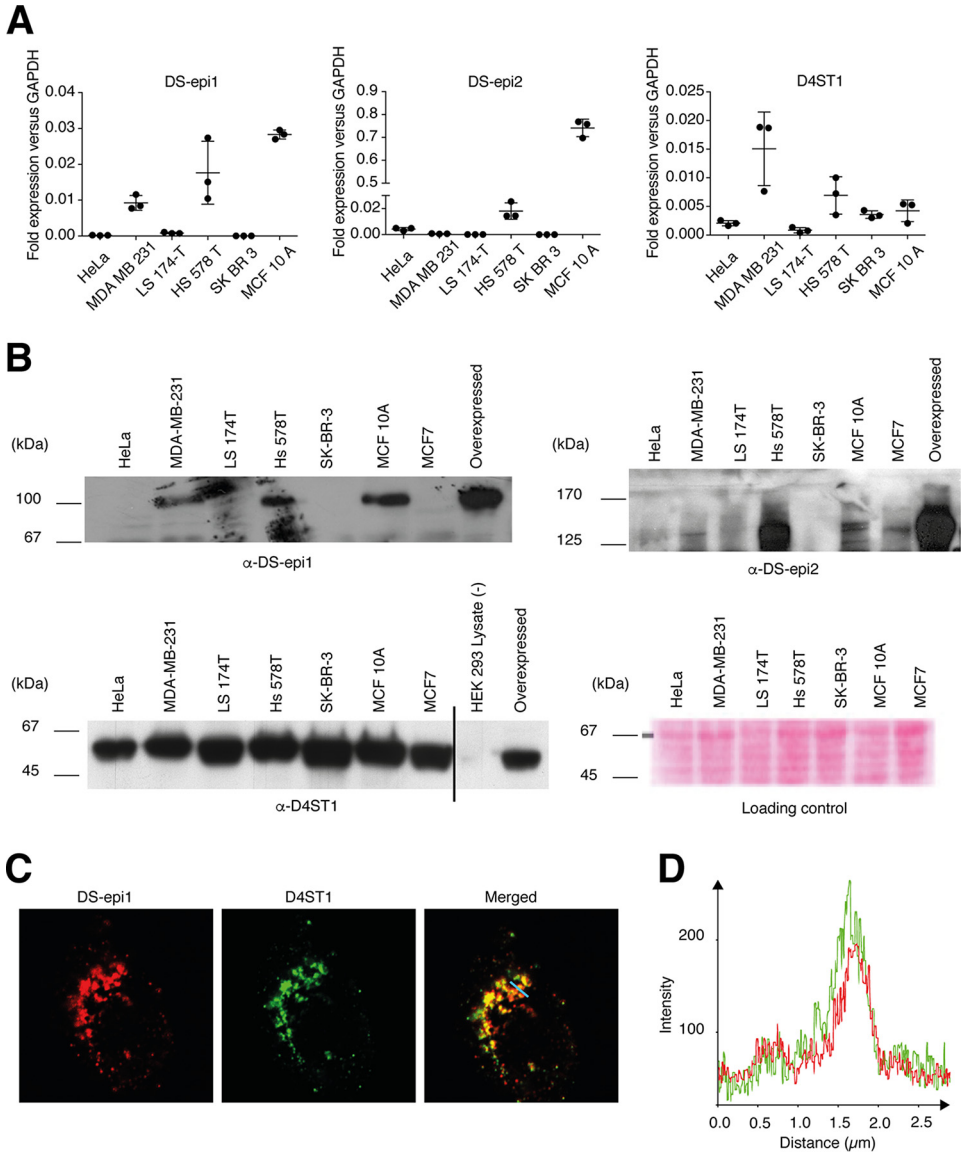

Figure 3. Endogenous DS-epi1 and D4ST1 colocalize in Golgi membranes. *A* and *B*, detection of DS-epi1, DS-epi2, and D4ST1 in cell lysates by qRT-PCR (*A*) (mean ± S.D.) and Western blotting (*B*). A *vertical line* splicing mark in the *lower left panel* indicates that some lanes of the original blot were not shown. *C*, confocal microscopy of MCF 10a cells after anti–DS-epi1 and anti-D4ST1 immunostaining. *D*, a line scan was performed in the section marked with a *blue line* in the merged view. Overlap of the two signals is apparent.

DS-epi2–specific siRNA in MCF 10a, resulting in 5% and ~10% remaining RNA and protein, respectively (Fig. 6, *A* and *B*). Unexpectedly, also DS-epi1 RNA and protein were reduced. To determine amount and distribution of IdoA in CS/DS chains, cells were ^{35}S-labeled and CS/DS was purified from the medium and the cell layer. Eighty-five percent of the recovered CS/DS was from the cell layer, which was further analyzed. Chain length was identical independent of the origin of control or DS-epi2–siRNA–treated cells (data not shown). CS/DS was cleaved by chondroitinase B, which cleave only sulfated GalNAc–IdoA linkages, and the size analysis of depolymerized material showed marked reduction of IdoA in all spatial arrangement (Fig. 6*C*). CS/DS chains obtained from control cells contained 39% of IdoA, which decreased to 11% after DS-epi2 down-regulation (Fig. 6*D*). Altogether, siRNA-mediated reduction of DS-epi2 in MCF 10a cells resulted in a marked reduction of the two epimerases and IdoA biosynthesis.

Discussion

The formation of CS/DS is a rapid process requiring at least 21 enzymes whose organization and kinetics are not well understood (19). Within CS/DS, the detailed structure and the length of IdoA-containing motifs are endowed with specific functions. For instance, a single or only a few IdoA–GalNAc–4*S* are sufficient for interaction with FGF-2, or the modulation of migration of neural crest cells, whereas interactions with heparin cofactor II require a hexasaccharide containing three 2-*O*-sulfated IdoA–GalNAc–4*S* moieties (11, 20–22). For collagen fibrillization, considerably longer blocks containing 4-*O*-sulfated GalNAc are required (23, 24). Regarding the formation of IdoA, DS-epi1, DS-epi2, and D4ST1 are the essential players, with DS-epi1 being the dominant epimerase in most tissues except for the brain, where DS-epi2 is the major enzyme (25). Using purified recombinant DS-epi1, in

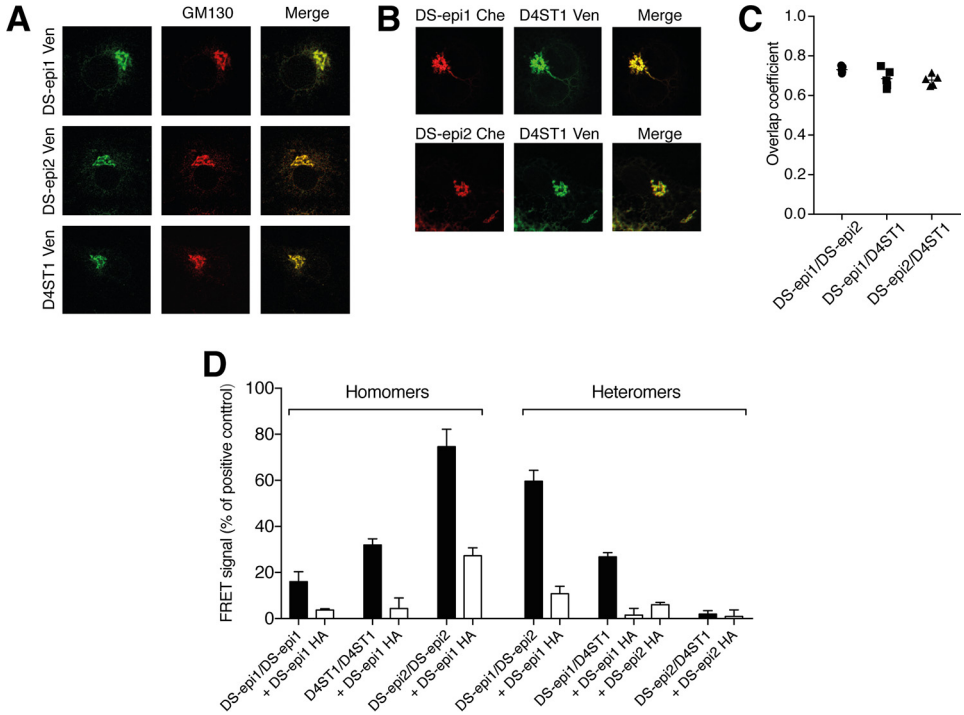

Figure 4. Colocalization of the D4ST1, DS-epi1, and DS-epi2 FRET constructs in transfected COS-7 cells and their mutual interactions. *A*, co-immunostaining of DS-epi1, DS-epi2, and D4ST1 mVenus constructs with the *cis*-Golgi marker protein GM130 in COS-7 cells visualized with a pseudocolored Alexa 405 secondary antibody. *B* and *C*, mutual colocalization of the three enzymes in the Golgi membranes and their overlap coefficients. The calculated average overlap coefficients of z-stacks (± S.D., $n = 5$) show over 65% overlap in the Golgi membranes with all three enzyme combinations tested. *D*, FRET interaction measurement. The FRET signal measured after co-expression of mCherry- or mVenus-enzyme constructs, alone or in combination with HA-tagged DS-epi1 or -epi2, is shown as indicated. FRET signals were normalized against the positive control values obtained by using the mVenus–mCherry fusion protein, which contains the transmembrane domain of β4GalT1 galactosyltransferase and a 30–amino acid linker region between the fluorescent proteins (37, 41). Each measurement was performed in 2–3000 cells/well, in six wells per transfection in triplicate. *Bars* represent the mean FRET signal (± S.D., no. of wells = 18).

the absence of D4ST1, only short IdoA-containing oligosaccharides from disaccharides to octasaccharides are formed (26). These structures are typically found in CS/DS-proteoglycans such as versican. In many other CS/DS proteoglycans, such as decorin, biglycan, CD44, and endocan, considerably longer blocks of IdoA–GalNAc–4*S* are present in a tissue-dependent manner.

In this report, we have shown a functional effect of the interplay between DS-epi1 and the IdoA-specific 4-*O*-sulfotransferase D4ST1. Co-incubation of DS-epi1 with D4ST1, in the presence of C5-^{3}H chondroitin, yielded a 5-fold larger release of ^{3}H, *i.e.* epimerase activity, compared with an incubation with DS-epi1 alone. Interestingly, disaccharide analysis of the products obtained after co-incubation showed that the reaction exhibited a lag phase where isolated or a few adjacent IdoA residues were produced followed by a phase where a full processive mode of action was displayed, allowing the synthesis of long IdoA–GalNAc–4-*O*-sulfated blocks. Possible explanations for these observations are an increase in substrate affinity upon initial modifications introduced by the two enzymes or an increased efficiency because of the direct interaction between the enzymes. We tested the second hypothesis by several different approaches. First, confocal microscopy showed that endogenously expressed DS-epi1 and D4ST1 largely colocalize in the Golgi of MCF 10a cells. Second, FRET experiments in COS-7 cells showed that DS-epi1 interacts with D4ST1. In addition, FRET revealed homomeric complexes of the three enzymes, confirmed by cellular cross-linking experiments, and that DS-epi2 interacts with DS-epi1, but not with D4ST1. The latter finding can be conceptualized by taking into consideration that DS-epi2 itself has a sulfotransferase domain, although its sulfotransferase activity has not yet been verified. It is thus plausible that DS-epi2 is self-sufficient regarding a coupled epimerase/sulfotransferase action. The formation of a heterocomplex DS-epi1/DS-epi2/D4ST1 was revealed by immunoprecipitation. The interaction between DS-epi2 and DS-epi1 indicates that DS-epi2 may participate in the formation/modulation of IdoA structures. This hypothesis was tested by siRNA-mediated down-regulation of DS-epi2 in MCF 10a cells. Unexpectedly, in addition to DS-epi2, also DS-epi1 was partially down-regulated. When DS-epi2 siRNA was analyzed by the supplier using their design algorithm, *DSE*, encoding DS-epi1, was not considered a potential off-target gene. Rather, we can speculate that DS-epi2 might be required for DS-epi1 stability, with unknown mechanisms. The resulting IdoA production in DS-epi2 down-regulated cells had a drastic 72% reduction. This result is in agreement with previous findings showing that DS-epi2 siRNA-mediated down-regulation in lung fibroblasts drastically reduced IdoA biosynthesis in medium-released decorin and versican CS/DS chains (3). However, the effect of *Dsel*, encoding DS-epi2, ablation in mice is much milder than in the studied cells. In fact, the two tissues with highest expression of DS-epi2, brain and kidney, had a 38 and 3% reduction of IdoA biosynthesis, respectively (25). In contrast to the MCF 10a cells, in *Dsel*$^{-/-}$ brain and kidney, DS-epi1 mRNA was slightly increased, emphasizing the fact that different compensatory

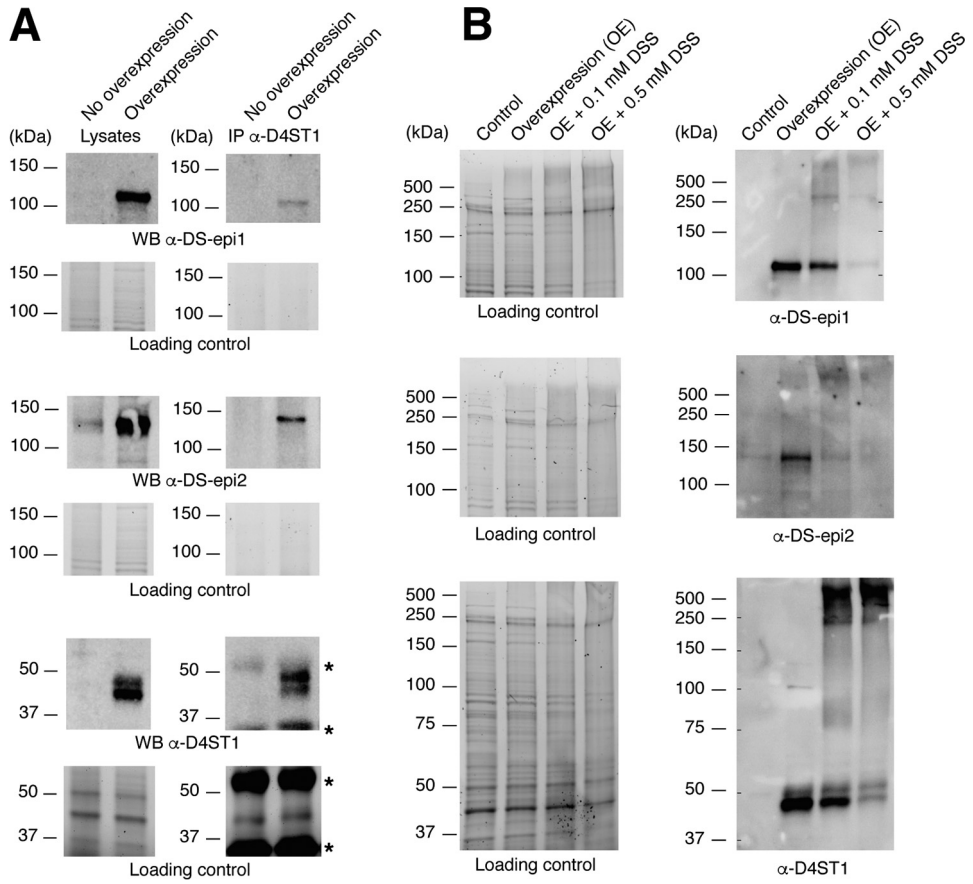

Figure 5. Formation of the DS-epi1/DS-epi2/D4ST1 complex and of high molecular weight complexes in COS-7. *A*, anti-D4ST1 immunoprecipitation of COS-7 lysates co-overexpressing the three enzymes; 8 μg of cell lysates or the immunoprecipitated material from starting 80 μg of lysate was applied. *Asterisk*, IgG heavy and light chains of the immunoprecipitating anti-D4ST1 antibody. *B*, cross-linking by disuccinimidyl suberate (*DSS*) of intact cells after single overexpression of the three enzymes. Western blots show that the enzymes, visible as monomers in the absence of cross-linker, are part of cross-linked high molecular weight complexes.

mechanisms might be at work in isolated cells and animal models. Clearly, the role of the DS-epi2/DS-epi1 complex requires further investigation, even though it is well established that DS-epi1 and -epi2 alone are epimerases, as revealed by the *Dsel* and *Dse* KO mice, respectively (23, 25).

The described functional and physical links between DS-epi1 and D4ST1 are in agreement with several lines of evidence and the intertwined relationship between epimerization and sulfation has been appreciated for a long time (27). Human mutations of *D4ST1* and *DSE* responsible for the musculocontractural type of Ehler-Danlos syndrome, abolish IdoA blocks in decorin produced by fibroblasts (7, 17). Similarly, siRNA down-regulation of the two genes in fibroblasts or *Dse* ablation in mice greatly down-regulates the production of IdoA blocks (3, 16, 23).

The notion of interactions between enzymes carrying out sequential reactions is known from other enzymatic systems in the CS/DS biosynthesis, where both linker-modifying enzymes, polymerases, and sulfotransferases have been shown to interact (28–31). In heparan sulfate biosynthesis, among other bimolecular interactions, C5-epimerase/2-*O*-sulfotransferase binding has been reported, where the two enzymes are dependent on each other for transport from the endoplasmic reticulum to the medial Golgi apparatus (32). The epimerization/2-*O*-sulfation in heparan sulfate clearly parallels the epimerization/4-*O*-sulfation in DS. The described DS-epi1/D4ST1 interaction does not disclose the organization of other enzymes involved in IdoA-containing structures during biosynthesis, such as the 2-*O*-sulfotransferase UST, which sulfates both GlcA and IdoA residues, or the GalNAc 4-sulfate 6-*O*-sulfotransferase, encoded by *CHST15*, which sulfates GalNAc-4*S* irrespective of the type of the adjacent uronic acid residue.

Finally, further studies on the molecular composition and Golgi localization of different biosynthetic complexes could explain the fine-tuning of the biosynthesis of the structurally diverse CS/DS. This knowledge could be transferred to biotechnological applications such as production of structurally defined recombinant CS/DS with pharmacological activities.

Experimental procedures

Materials

PAPS was prepared from ATP using ATP sulfurylase, APS kinase, and pyrophosphatase as described previously (33). (Enzymes were a kind gift from professor Jian Liu, University of North Carolina at Chapel Hill.) Chondroitin (Ch) and [5-^{3}H]Ch were prepared by defructosylation of the K4 polysaccharide as described previously (34).

Cloning and expression of recombinant DS-epi1 and D4ST1

DS-epi1 was cloned, expressed, and purified as previously described (26). The portion of the ORF of the human dermatan

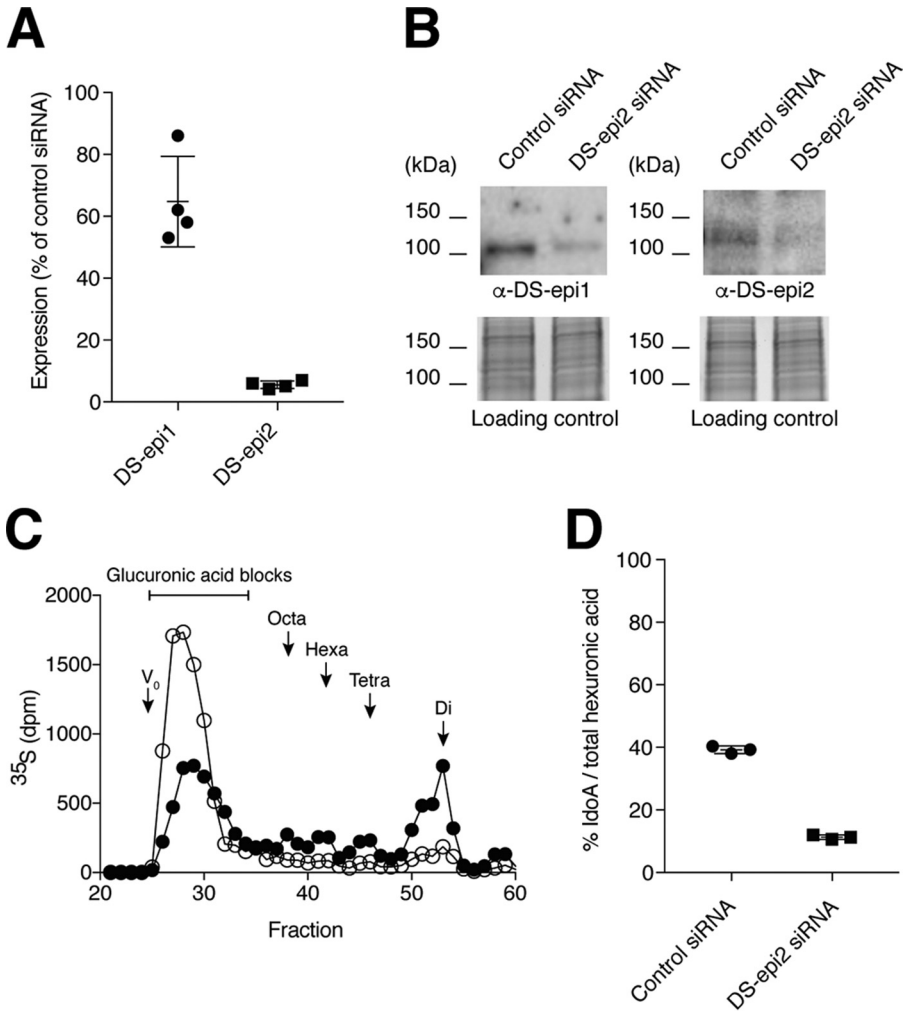

Figure 6. Down-regulation of DS-epi2 in MCF 10a cells results in decrease of both epimerases and IdoA content in CS/DS chains. *A* and *B*, after DS-epi2 down-regulation by siRNA in MCF 10a cells, (*A*) DS-epi2 and DS-epi1 RNA were quantified by qRT-PCR; data are expressed relative to the control siRNA and normalized to GAPDH expression (mean ± S.D.); and (*B*) proteins were visualized by Western blotting. *C*, cells were labeled by ^{35}S, and the resulting purified ^{35}S-CS/DS chains were depolymerized with chondroitinase B and applied to a Superdex Peptide size-permeation column. *Filled circles*, control siRNA; *empty circles*, DS-epi2 siRNA. *D*, from the size pattern in *C*, content of IdoA was calculated (mean ± S.D.).

4-*O*-sulfotransferase 1, in short *D4ST1* gene (*CHST14*, NM_130468.3, cDNA) corresponding to amino acids 61 to 376 was subcloned together with a C-terminal His_8 tag into the NheI and NotI sites of the pCEP-Pu/BM40 (35) expression vector using the following primers (Sigma-Aldrich): forward (NheI restriction site is indicated in bold): amino acid (aa) 61, 5′-GCATCT**GCTAGC**CGAGCGGGGCATCCTGGCCGAGATGAA-3′; reverse (NotI restriction site is indicated in bold): aa 376, 5′-GCATCT**GCGGCCGC**GTCAATGG TGATGGTGATGATGGTGGTGCTGCTGACACGCCTCCTT-3′. Transfection, expression, and protein purification were performed as previously described (26). After Ni-NTA affinity purification of conditioned growth medium, the protein yield was ~2 mg/liter of growth medium.

Isolation of monomeric protein fractions

DS-epi1 and D4ST1 were separated on a Superose 12 10/300 column (GE Healthcare Life Sciences) using running buffer composed of HEPES (20 mM, pH 7.9), NaCl (150 mM), and $MnCl_2$ (2 mM). The column was operated at 0.5 ml/min and monomeric fractions were pooled and concentrated using 10 kDa MWCO Amicon Ultra centrifugal concentrators (EMD Millipore).

Enzymatic incubations of DS-epi1 and D4ST1

DS-epi1 (1 μg, final concentration 110 nM) was incubated with [5-^{3}H]chondroitin (~1 μg, 25,000 dpm) and PAPS (final concentration 0.3 mM) in a total volume of 100 μl MES buffer (20 mM, pH 6.0) supplemented with $MnCl_2$ (10 mM), $MgCl_2$ (5 mM), and 10 μg BSA. D4ST1 (1.7 μg, final concentration 380 nM) was added for the co-incubation experiments and PAP^{35}S (1 μCi) was added to study the spatial distribution of the IdoA–GalNAc–4*S* moieties (Fig. 2). After incubation at 37 °C, the samples were boiled and subsequently centrifuged at 20,000 × *g* for 5 min. The supernatant contained both the unmodified tritiated polysaccharide substrate and tritiated water, formed as the coproduct of epimerase activity, which was isolated by distillation and measured with liquid scintillation counting. Alternatively, the supernatant was processed for disaccharide analysis.

Disaccharide analysis

Samples were buffer-exchanged into ammonium acetate buffer (50 mM, pH 7.5) using 3 kDa MWCO Amicon Ultra centrifugal concentrators (EMD Millipore). Chondroitinase ABC (10 mIU, Sigma-Aldrich) was added to each sample (~30 μl) to depolymerize the polysaccharide products to $\Delta^{4,5}$-unsaturated uronic acid–containing disaccharides. Depolymerization was achieved by incubation at 37 °C for 4 h, after which the samples were boiled and centrifuged at 20,000 × *g* for 10 min, and the supernatant was dried. CS/DS disaccharides, labeled by 2-aminoacridone, were analyzed on a Thermo Fisher Scientific UltiMate 3000 Quaternary Analytical System equipped with an FLD-3400RS fluorescence detector as described previously (36). Disaccharide standards were obtained from Iduron (Manchester, UK).

Size determination of enzymatic products

GAG samples (~3 μg) from the enzymatic assays were degraded overnight at 37 °C with chondroitinase AC-I and -II (5 mIU each, AMS Biotechnology) in 50 μl of ammonium acetate buffer (50 mM, pH 8.0). Degraded samples were separated using a Superdex Peptide 10/300 column (GE Healthcare Life Sciences) using ammonium bicarbonate (0.2 M) at 0.3 ml/min as the running buffer. Eluted fractions were analyzed by liquid scintillation counting.

RNA isolation and gene expression quantification by qRT-PCR

Total RNA was extracted using the RNeasy Mini Kit (Qiagen) and reverse transcribed to cDNA (Quantitect Reverse Transcription Kit, Qiagen). Real-time quantitative PCR was run using the Fast SYBR Green Master Mix (Ambion Life Technologies) and the Mx3005P qPCR system (Stratagene) with standard cycling parameters. The -fold expression values were calculated using the $2^{-\Delta Ct}$ formula, using the housekeeping gene GAPDH as control. The sequences of the primers were: DS-epi1: forward 5′-GAGTCCCTTGGAGACAGCAG-3′ and reverse 5′-GCCAGTATCGTCCATCCAGT-3′; DS-epi2: forward 5′-TCTGGTATGATCCCCAGCTC-3′ and reverse 5′-ACCCAGCCCCATAAGTAACC-3′; D4ST1: forward 5′-ATTCCCCGAGTTCCTGAGAT-3′ and reverse 5′-CAGCCTCCAGCCTCTCATAG-3′; GAPDH: forward 5′-GAAGGTGAAGGTCGGAGTCA-3′ and reverse 5′-TGGAAGATGGTGATGGGATT-3′.

Western blotting

Protein concentration was determined in cleared lysates by Bradford method (Bio-Rad), using BSA as standard. Anti–DS-epi1 used for Fig. 3 was from Sigma-Aldrich (HPA014764) and for Figs. 5 and 6 an antigen-purified rabbit polyclonal antibody obtained after antigen peptide immunization (KWSKYKHDLAAS corresponding to amino acids 509–520 of the human/murine sequence) from Innovagen. Anti–DS-epi2 was an antigen-purified rabbit polyclonal antibody (antigen FDRDAEYIRALRRH corresponding to amino acids 978–991), from Innovagen. Anti-D4ST1 used for Fig. 3 was from Santa Cruz Biotechnology (V18), and for Fig. 5 an antigen-purified rabbit polyclonal antibody (antigen PGREGTAWRGKAPK corresponding to amino acids 76–89) from Innovagen. Anti–species-specific HRP-conjugated IgG were the secondary reagents, detected with the ECL substrate SuperSignal® West Dura (Thermo Fisher Scientific). Loading control was visualized in Stain Free Gels (Bio-Rad). Images were taken with the Chemi-Doc Touch Imaging System (Bio-Rad).

Cloning of plasmid constructs for FRET experiments

Plasmids for FRET experiments were all based on a pcDNA3 vector backbone (Invitrogen) and the constructs were prepared from full-length cDNA clones (*DSE*, encoding DS-epi1: NCBI NM_013352.3; *DSEL*, encoding DS-epi2: NCBI NM_032160.2; *D4ST1*: NCBI NM_130468.3). See Fig. 1 for an overview of the constructs used in this study. For the *DSE* and *DSEL* FRET plasmids, monomeric Cherry (mCherry) and Venus (mVenus) were subcloned together with the signal peptide of DS-epi1 (amino acids 1–22) using the following primers: forward (HindIII), 5′-CAC**AAGCTT**ACCATGAGGACTCACACACGGGGGGCT CCCAGTGTGTTTTTCATATATTTGCTTTGCTTTGTGTCAGCCTACATGGTGAGCAAGGGCGAGG-3′ and reverse (NotI), 5′-GTG**GCGGCCGC**GGCGACCGGCTTGTACAGCTCGTCCATGCC-3′. The DNA encoding amino acids 23–958 of DS-epi1 were subcloned downstream of mCherry/mVenus using the following primers: forward (EcoRI), 5′-TAATAT**GAATTC**ATGTTCCCCCGCCCGCTGACC-3′ and reverse (XbaI), 5′-GTGTT**TCTAGA**CTGCTGACACGCCTCCTTGGTGAC-3′. The DNA encoding amino acids 21–1212 of DS-epi2 were subcloned downstream of mCherry/mVenus using the following primers: forward (NotI), 5′-GCATCT**GCGGCCGC**TACTTTTGAGGAATCTGTGAGCA-3′ and reverse (XbaI), 5′-GCATCT**TCTAGA**TTAGTCCATAAACTTTGGAT-3′.

For *D4ST1*, mCherry and mVenus were subcloned into the pcDNA3 vector as previously described (37, 38). The DNA encoding amino acids 1–376 of D4ST1 were subcloned upstream of mCherry/mVenus using the following primers: forward (EcoRI), 5′-TAATAT**GAATTC**ATGTTCCCCCGCCCGCTGACC-3′ and reverse (XbaI), 5′-GTGTT**TCTAGA**CTGCTGACACGCCTCCTTGGTGAC-3′.

HA-tagged *DSE* and *DSEL* were constructed by inserting the DNA encoding amino acids 1–958 and 1–1222, respectively, C-terminally from the HA sequence in the pcDNA3 vector using the following primers: *DSE* forward (XhoI), 5′-ATAAT**CTCGAG**ATGAGGACTCACACACGGGGGGC-3′ and reverse (XbaI), 5′-GTGTT**TCTAGA**ACACTGTGATTGGGAACAAGAAGAGTACAACC-3′; *DSEL* forward (XhoI), 5′-AATA**CTCGAG**ATGCCTAAGGGAGGAGCTCCCCCATG-3′ and reverse (XbaI), 5′-ACCACC**TCTAGA**GTCCATAAACTTTGGATATCCTAGGCGATCCATC-3′.

Confocal microscopy

MCF 10a cells were plated onto coverslips (NUNC, Thermo Scientific) and grown at 37 °C in a 5% CO_2 incubator until 50–80% confluency in DMEM/F12 (Thermo Fisher Scientific) supplemented with 5% horse serum, penicillin/streptomycin, glutamine, 20 ng/ml epithelial growth factor, 0.1 μg/ml cholera toxin, 10 μg/ml insulin, and 0.5 μg/ml hydrocortisone. Coverslips were washed briefly with PBS and fixed for 2 min with

ice-cold methanol at −20 °C. Cells were then washed with PBS and permeabilized by a 10-min incubation with 0.2% Triton in PBS at room temperature. Unspecific site blocking was performed for 2 h with 5% BSA in PBS. Subsequently, coverslips were incubated (incubation and wash buffer was 1% BSA in PBS) overnight with primary antibodies (diluted 1:100). After washing, goat anti-human D4ST1 (Santa Cruz Biotechnology, V-18) and rabbit anti-human DS-epi1 (Sigma-Aldrich, anti-SART2) were used at a dilution of 1:100. Cells were washed and incubated for 30 min with the secondary antibodies Alexa Fluor 488 and Alexa Fluor 633 (diluted 1:200). Images were acquired on a Zeiss 710 confocal microscope (Carl Zeiss GmbH, Jena, Germany) equipped with a diode laser (405 nm), an argon laser (488 nm), and two helium-neon lasers (543 nm and 633 nm). All images were acquired at Nyquist resolution (70 nm/pixel), as recommended by the manufacturer, using an 63× numerical aperture (NA) 1.4 oil immersion Plan-Apochromat objective lens. To minimize noise, a line averaging 4 and a pinhole of 1.0 were used.

COS-7 cells were grown in DMEM as previously described (39). Briefly, cells were grown in 5% CO_2 at 37 °C in high-glucose DMEM (Thermo Fisher) on 9.6 cm^2 culture dishes (Greiner CELLSTAR 627170). One day after plating, the cells were transfected using 0.5 μg of each plasmid cDNA and FuGENE 6® transfection reagent according to the supplier's protocol (Promega, Madison, WI). Twenty-four h post transfection, cells were processed either for fluorescence microscopy or FRET measurements (see below). Immunofluorescence samples were fixed with 4% PFA for 20 min before blocking the cells with 1% BSA in PBS (pH 7.4) supplemented with 0.05% saponin for 1 h. When appropriate, the samples were then costained with primary anti-GM130 (clone 35, BD Biosciences) and secondary anti-mouse Alexa Fluor 405 antibodies (Thermo Fisher). Cells were imaged with a 63× oil immersion objective (numerical aperture 1.4) with a Zeiss LSM 700 confocal microscope and Zen 2009 software. Z-stacks were acquired from each image to calculate the colocalization coefficients with the built-in colocalization analysis module (average overlap coefficient of the z-stack ± S.D., $n = 5$).

High-content FRET measurements and quantification

Twenty-four h after transfection, cells expressing both mVenus (mVen, donor) and mCherry (mChe, acceptor) constructs were transferred onto PerkinElmer CellCarrier Ultra 96-well plates with 10,000 cells per well. After 6 h, attached cells were fixed with 4% PFA and washed with PBS (pH 7.4). Samples were imaged on a PerkinElmer Operetta high-content imager with appropriate filter sets for mVenus, mCherry, and FRET. Analysis was performed with built-in Harmony 4.6 software using the Youvan FRET formula. Data are shown as the average FRET signal from 2–3000 cells/well, performed in 6 wells per transfection in triplicates (± S.D., no. of wells = 18) (40).

Immunoprecipitation

DS-epi1, DS-epi2, and D4ST1 were co-overexpressed in COS-7 cells. The plasmid DNAs were HA–DS-epi1, as previously described. Sequence harmonized human DS-epi2 DNA (GenScript) corresponding to amino acids 31 to 1222 was subcloned into the NheI and NotI sites of the pCEP-Pu/BM40 expression vector using the following primers (Sigma-Aldrich): forward (NheI restriction site is indicated in bold): amino acid (aa) 31, 5′-GCATCT**GCTAGC**CACCTTTGAAGAATCCGTGAGCAAC-3′ and reverse (NotI restriction site is indicated in bold) aa 1222, 5′-GCATCT**GCGGCCGC**GTCCATGAACTTGGGATAGCC-3′. *D4ST1-HA* was constructed by inserting DNA encoding the full-size 1–376 D4ST1 N-terminally from the HA sequence in the pcDNA3 vector using the following primers: forward, TAATAT**CTCGAG**ATGTTCCCCCGCCCGCTGACC (XhoI restriction site indicated in bold); reverse GTGTT**TCTAGA**CTGCTGACACGCCTCCTTGGTGAC (XbaI). The transfection reagent FuGENE® HD was used according to the supplier's protocol (Promega).

Forty-eight h after transfection, cells were washed with PBS and lysed in 50 mM Tris, pH 8.0, 150 mM NaCl, 1% Triton, 1 mM DTT, cOmplete Protease Inhibitor tablets (Roche). Three hundred μg lysate was pre-cleared with the rabbit Ig IP beads (Rockland Immunochemicals, 00–8800-25), and 2 μg anti-D4ST1 antibodies (immunogen sequence: amino acids 76–89) was added. The IgG were pulled down with the rabbit Ig IP beads, which were subsequently washed in lysis buffer. Western blotting utilized as secondary reagent the anti-rabbit native IgG HRP-conjugated reagent, which recognizes the IgG used for immunodetection, which are in native form, and not the IgG used for precipitation, denatured by Laemmli buffer (Rockland Immunochemicals, 18-8816-31).

Cross-linking

DS-epi1, DS-epi2, and D4ST1 were individually overexpressed in COS-7 cells as above. Forty-eight h after transfection, cells were washed with PBS and kept at room temperature for 30 min covered with a solution of disuccinimidyl suberate (Thermo Fisher) cross-linker (dissolved at 50 mM in DMSO and then to 0.1 and 0.5 mM in PBS). The cross-linker was quenched by adding Tris, pH 7.5, at a final concentration of 20 mM for an additional 15 min. Cells were washed with PBS and lysed in a buffer containing 20 mM MES, pH 6.5, 150 mM NaCl, 10% glycerol, 1 mM DTT, 1 mM EDTA, 1% Triton X-100, cOmplete Protease Inhibitor tablets (Roche).

siRNA-mediated down-regulation of DS-epi2 and iduronic acid analysis

MCF 10a cells were reverse-transfected with 20 nM of DS-epi2–specific siRNA or control siRNA complexed with the transfection reagent Lipofectamine® RNAiMax (Invitrogen), used according to the manufacturer's protocol. The DS-epi2 siRNA sequence was 5′-GGAUGGUUGGCUACAAAGAtt-3′ (i.d. 33832; negative control AM4611; both from Ambion), whose potency was previously verified and compared with another sequence (3). After 48 h, normal culturing medium was substituted with labeling medium (sulfate-free DMEM (Gibco), supplemented with 5% horse serum, penicillin/streptomycin, glutamine, 20 ng/ml epithelial growth factor, 0.1 μg/ml cholera toxin, 10 μg/ml insulin, and 0.5 μg/ml hydrocortisone) which included 100 μCi/ml ^{35}S (Perkin Elmer) and freshly added 20 nM DS-epi2/control siRNA-transfection reagent complexes.

After 24 h cells and medium were protease- and DNase-digested, and GAGs were purified on DE52 anion-exchange chromatography. Heparan sulfate chains were degraded by deamination at pH 1.5, and the CS/DS chains were recovered from Superose 6 columns run in 0.2 M ammonium bicarbonate. The purity of labeled CS/DS was ascertained by degradation to disaccharides by chondroitinase ABC (Sigma-Aldrich, C3667). Quantification and spatial arrangement of IdoA along the chain was analyzed by cleaving 20,000 dpm of CS/DS with 2 mIU of chondroitinase B (R&D Systems) in 20 mM HEPES, pH 7.2, 50 mM NaCl, 4 mM $CaCl_2$, and 0.1 mg/ml BSA overnight at 37 °C. The split products were separated on a Superdex Peptide column (GE Healthcare Life Sciences) run in 0.2 M ammonium bicarbonate.

Statistical analyses

Statistical analyses were performed using Student's *t* test for the comparison of small, normally distributed samples.

Author contributions—E. T., A. H., M. A. T., A. M., S. K., and M. M. conceptualization; E. T., A. H., K. Z., A. M., S. K., and M. M. data curation; E. T., A. H., A. M., S. K., and M. M. formal analysis; E. T., A. H., K. Z., M. A. T., G. F., U. E., G. W.-T., A. M., S. K., and M. M. investigation; E. T., A. H., and M. M. methodology; E. T., A. H., A. M., S. K., and M. M. writing-original draft; E. T., A. H., K. Z., M. A. T., G. F., U. E., G. W.-T., A. M., S. K., and M. M. writing-review and editing; A. M. and M. M. supervision; A. M. and M. M. funding acquisition.

Acknowledgment—We thank Hinke Multhaupt for advice on confocal microscopy.

References

1. Malmström, A., Bartolini, B., Thelin, M. A., Pacheco, B., and Maccarana, M. (2012) Iduronic acid in chondroitin/dermatan sulfate: Biosynthesis and biological function. *J. Histochem. Cytochem.* **60,** 916–925 CrossRef Medline
2. Maccarana, M., Olander, B., Malmström, J., Tiedemann, K., Aebersold, R., Lindahl, U., Li, J.-P., and Malmström, A. (2006) Biosynthesis of dermatan sulfate: Chondroitin-glucuronate C5-epimerase is identical to SART2. *J. Biol. Chem.* **281,** 11560–11568 CrossRef Medline
3. Pacheco, B., Malmström, A., and Maccarana, M. (2009) Two dermatan sulfate epimerases form iduronic acid domains in dermatan sulfate. *J. Biol. Chem.* **284,** 9788–9795 CrossRef Medline
4. Mikami, T., Mizumoto, S., Kago, N., Kitagawa, H., and Sugahara, K. (2003) Specificities of three distinct human chondroitin/dermatan *N*-acetylgalactosamine 4-*O*-sulfotransferases demonstrated using partially desulfated dermatan sulfate as an acceptor: Implication of differential roles in dermatan sulfate biosynthesis. *J. Biol. Chem.* **278,** 36115–36127 CrossRef Medline
5. Thelin, M. A., Bartolini, B., Axelsson, J., Gustafsson, R., Tykesson, E., Pera, E., Oldberg, Å., Maccarana, M., and Malmström, A. (2013) Biological functions of iduronic acid in chondroitin/dermatan sulfate. *FEBS J.* **280,** 2431–2446 CrossRef Medline
6. Kosho, T. (2016) CHST14/D4ST1 deficiency: New form of Ehlers-Danlos syndrome. *Pediatr. Int.* **58,** 88–99 CrossRef Medline
7. Müller, T., Mizumoto, S., Suresh, I., Komatsu, Y., Vodopiutz, J., Dundar, M., Straub, V., Lingenhel, A., Melmer, A., Lechner, S., Zschocke, J., Sugahara, K., and Janecke, A. R. (2013) Loss of dermatan sulfate epimerase (DSE) function results in musculocontractural Ehlers-Danlos syndrome. *Hum. Mol. Genet.* **22,** 3761–3772 CrossRef Medline
8. Syx, D., Van Damme, T., Symoens, S., Maiburg, M. C., van de Laar, I., Morton, J., Suri, M., Del Campo, M., Hausser, I., Hermanns-Lê, T., De Paepe, A., and Malfait, F. (2015) Genetic heterogeneity and clinical variability in musculocontractural Ehlers-Danlos syndrome caused by impaired dermatan sulfate biosynthesis. *Hum. Mutat.* **36,** 535–547 CrossRef Medline
9. Thelin, M. A., Svensson, K. J., Shi, X., Bagher, M., Axelsson, J., Isinger-Ekstrand, A., van Kuppevelt, T. H., Johansson, J., Nilbert, M., Zaia, J., Belting, M., Maccarana, M., and Malmström, A. (2012) Dermatan sulfate is involved in the tumorigenic properties of esophagus squamous cell carcinoma. *Cancer Res.* **72,** 1943–1952 CrossRef Medline
10. He, L., Giri, T. K., Vicente, C. P., and Tollefsen, D. M. (2008) Vascular dermatan sulfate regulates the antithrombotic activity of heparin cofactor II. *Blood* **111,** 4118–4125 CrossRef Medline
11. Taylor, K. R., Rudisill, J. A., and Gallo, R. L. (2005) Structural and sequence motifs in dermatan sulfate for promoting fibroblast growth factor-2 (FGF-2) and FGF-7 activity. *J. Biol. Chem.* **280,** 5300–5306 CrossRef Medline
12. Deakin, J. A., Blaum, B. S., Gallagher, J. T., Uhrín, D., and Lyon, M. (2009) The binding properties of minimal oligosaccharides reveal a common heparan sulfate/dermatan sulfate-binding site in hepatocyte growth factor/scatter factor that can accommodate a wide variety of sulfation patterns. *J. Biol. Chem.* **284,** 6311–6321 CrossRef Medline
13. Catlow, K. R., Deakin, J. A., Wei, Z., Delehedde, M., Fernig, D. G., Gherardi, E., Gallagher, J. T., Pavão, M. S. G., and Lyon, M. (2008) Interactions of hepatocyte growth factor/scatter factor with various glycosaminoglycans reveal an important interplay between the presence of iduronate and sulfate density. *J. Biol. Chem.* **283,** 5235–5248 CrossRef Medline
14. Dick, G., Grøndahl, F., and Prydz, K. (2008) Overexpression of the 3′-phosphoadenosine 5′-phosphosulfate (PAPS) transporter 1 increases sulfation of chondroitin sulfate in the apical pathway of MDCK II cells. *Glycobiology* **18,** 53–65 CrossRef Medline
15. Kellokumpu, S., Hassinen, A., and Glumoff, T. (2016) Glycosyltransferase complexes in eukaryotes: Long-known, prevalent but still unrecognized. *Cell. Mol. Life Sci.* **73,** 305–325 CrossRef Medline
16. Pacheco, B., Maccarana, M., and Malmström, A. (2009) Dermatan 4-*O*-sulfotransferase 1 is pivotal in the formation of iduronic acid blocks in dermatan sulfate. *Glycobiology* **19,** 1197–1203 CrossRef Medline
17. Miyake, N., Kosho, T., Mizumoto, S., Furuichi, T., Hatamochi, A., Nagashima, Y., Arai, E., Takahashi, K., Kawamura, R., Wakui, K., Takahashi, J., Kato, H., Yasui, H., Ishida, T., Ohashi, H., *et al.* (2010) Loss-of-function mutations of CHST14 in a new type of Ehlers-Danlos syndrome. *Hum. Mutat.* **31,** 966–974 CrossRef Medline
18. Pacheco, B., Maccarana, M., Goodlett, D. R., Malmström, A., and Malmström, L. (2009) Identification of the active site of DS-epimerase 1 and requirement of *N*-glycosylation for enzyme function. *J. Biol. Chem.* **284,** 1741–1747 CrossRef Medline
19. Mikami, T., and Kitagawa, H. (2013) Biosynthesis and function of chondroitin sulfate. *Biochim. Biophys. Acta* **1830,** 4719–4733 CrossRef Medline
20. Radek, K. A., Taylor, K. R., and Gallo, R. L. (2009) FGF-10 and specific structural elements of dermatan sulfate size and sulfation promote maximal keratinocyte migration and cellular proliferation. *Wound Repair Regen.* **17,** 118–126 CrossRef Medline
21. Maimone, M. M., and Tollefsen, D. M. (1990) Structure of a dermatan sulfate hexasaccharide that binds to heparin cofactor II with high affinity. *J. Biol. Chem.* **265,** 18263–18271 Medline
22. Gouignard, N., Maccarana, M., Strate, I., von Stedingk, K., Malmström, A., and Pera, E. M. (2016) Musculocontractural Ehlers-Danlos syndrome and neurocristopathies: Dermatan sulfate is required for *Xenopus* neural crest cells to migrate and adhere to fibronectin. *Dis. Models Mech.* **9,** 607–620 CrossRef Medline
23. Maccarana, M., Kalamajski, S., Kongsgaard, M., Magnusson, S. P., Oldberg, Å., and Malmström, A. (2009) Dermatan sulfate epimerase 1-deficient mice have reduced content and changed distribution of iduronic acids in dermatan sulfate and an altered collagen structure in skin. *Mol. Cell. Biol.* **29,** 5517–5528 CrossRef Medline
24. Fransson, L. A., Cöster, L., Malmström, A., and Sheehan, J. K. (1982) Self-association of scleral proteodermatan sulfate. Evidence for interaction via the dermatan sulfate side chains. *J. Biol. Chem.* **257,** 6333–6338 Medline

25. Bartolini, B., Thelin, M. A., Rauch, U., Feinstein, R., Oldberg, Å., Malmström, A., and Maccarana, M. (2012) Mouse development is not obviously affected by the absence of dermatan sulfate epimerase 2 in spite of a modified brain dermatan sulfate composition. *Glycobiology* **22,** 1007–1016 CrossRef Medline
26. Tykesson, E., Mao, Y., Maccarana, M., Pu, Y., Gao, J., Lin, C., Zaia, J., Westergren-Thorsson, G., Ellervik, U., Malmström, L., and Malmström, A. (2016) Deciphering the mode of action of the processive polysaccharide modifying enzyme dermatan sulfate epimerase 1 by hydrogen-deuterium exchange mass spectrometry. *Chem. Sci.* **7,** 1447–1456 CrossRef Medline
27. Eklund, E., Rodén, L., Malmström, M., and Malmström, A. (2000) Dermatan is a better substrate for 4-*O*-sulfation than chondroitin: Implications in the generation of 4-*O*-sulfated, L-iduronate-rich galactosaminoglycans. *Arch. Biochem. Biophys.* **383,** 171–177 CrossRef Medline
28. Kitagawa, H., Izumikawa, T., Uyama, T., and Sugahara, K. (2003) Molecular cloning of a chondroitin polymerizing factor that cooperates with chondroitin synthase for chondroitin polymerization. *J. Biol. Chem.* **278,** 23666–23671 CrossRef Medline
29. Izumikawa, T., Koike, T., Shiozawa, S., Sugahara, K., Tamura, J.-I., and Kitagawa, H. (2008) Identification of chondroitin sulfate glucuronyltransferase as chondroitin synthase-3 involved in chondroitin polymerization. *J. Biol. Chem.* **283,** 11396–11406 CrossRef Medline
30. Izumikawa, T., Koike, T., and Kitagawa, H. (2012) Chondroitin 4-*O*-sulfotransferase-2 regulates the number of chondroitin sulfate chains initiated by chondroitin *N*-acetylgalactosaminyltransferase-1. *Biochem. J.* **441,** 697–705 CrossRef Medline
31. Izumikawa, T., Sato, B., Mikami, T., Tamura, J.-I., Igarashi, M., and Kitagawa, H. (2015) GlcUAβ1–3Galβ1–3Galβ1–4xyl(2-*O*-phosphate) is the preferred substrate for chondroitin *N*-acetylgalactosaminyltransferase-1. *J. Biol. Chem.* **290,** 5438–5448 CrossRef Medline
32. Pinhal, M. A., Smith, B., Olson, S., Aikawa, J., Kimata, K., and Esko, J. D. (2001) Enzyme interactions in heparan sulfate biosynthesis: Uronosyl 5-epimerase and 2-*O*-sulfotransferase interact *in vivo*. *Proc. Natl. Acad. Sci. U.S.A.* **98,** 12984–12989 CrossRef Medline
33. Zhou, X., Chandarajoti, K., Pham, T. Q., Liu, R., and Liu, J. (2011) Expression of heparan sulfate sulfotransferases in *Kluyveromyces lactis* and preparation of 3′-phosphoadenosine-5′-phosphosulfate. *Glycobiology* **21,** 771–780 CrossRef Medline
34. Hannesson, H. H., Hagner-McWhirter, A., Tiedemann, K., Lindahl, U., and Malmstrom, A. (1996) Biosynthesis of dermatan sulphate. Defructosylated *Escherichia coli* K4 capsular polysaccharide as a substrate for the D-glucuronyl C-5 epimerase, and an indication of a two-base reaction mechanism. *Biochem. J.* **313,** 589–596 Medline
35. Kohfeldt, E., Maurer, P., Vannahme, C., and Timpl, R. (1997) Properties of the extracellular calcium binding module of the proteoglycan testican. *FEBS Lett.* **414,** 557–561 CrossRef Medline
36. Stachtea, X. N., Tykesson, E., van Kuppevelt, T. H., Feinstein, R., Malmström, A., Reijmers, R. M., and Maccarana, M. (2015) Dermatan sulfate-free mice display embryological defects and are neonatal lethal despite normal lymphoid and non-lymphoid organogenesis. *PLoS One* **10,** e0140279 CrossRef Medline
37. Hassinen, A., Pujol, F. M., Kokkonen, N., Pieters, C., Kihlström, M., Korhonen, K., and Kellokumpu, S. (2011) Functional organization of Golgi *N*- and *O*-glycosylation pathways involves pH-dependent complex formation that is impaired in cancer cells. *J. Biol. Chem.* **286,** 38329–38340 CrossRef Medline
38. Hassinen, A., and Kellokumpu, S. (2014) Organizational interplay of Golgi *N*-glycosyltransferases involves organelle microenvironment-dependent transitions between enzyme homo- and heteromers. *J. Biol. Chem.* **289,** 26937–26948 CrossRef Medline
39. Kokkonen, N., Rivinoja, A., Kauppila, A., Suokas, M., Kellokumpu, I., and Kellokumpu, S. (2004) Defective acidification of intracellular organelles results in aberrant secretion of cathepsin D in cancer cells. *J. Biol. Chem.* **279,** 39982–39988 CrossRef Medline
40. Youvan, D. C., Silva, C. M., Bylina, E. J., Coleman, W. J., Dilwort, M. R., and Yang, M. M. (1997) Calibration of fluorescence resonance energy transfer in microscopy using genetically engineered GFP derivatives on nickel chelating beads. *Biotechnol. et alia* **3,** 1–18
41. Llopis, J., McCaffery, J. M., Miyawaki, A., Farquhar, M. G., and Tsien, R. Y. (1998) Measurement of cytosolic, mitochondrial, and Golgi pH in single living cells with green fluorescent proteins. *Proc. Natl. Acad. Sci. U.S.A.* **95,** 6803–6808 CrossRef Medline